Acta Cryst E CRYSTALLOGRAPHIC COMMUNICATIONS

ISSN 2056-9890

Crystal structure, Hirshfeld surface analysis, intermolecular interaction energies, energy frameworks and DFT calculations of 4-amino-1-(prop-2-yn-1-yl)pyrimidin-2(1*H*)-one

Mouad Lahyaoui,[a]* Amal Haoudi,[b] Badr Eddine Kartah,[c] Ahmed Mazzah,[d] Tuncer Hökelek,[e] Joel T. Mague,[f] Youssef Kandri Rodi[g] and Nada Kheira Sebbar[h,c]

[a]Laboratoire de Chimie Organique Appliquée, Université Sidi Mohamed Ben Abdallah, Faculté des Sciences et Techniques, Route d'Immouzzer, BP 2202 Fez, Morocco, [b]Laboratory Of Applied Organic Chemistry, Sidi Mohamed Ben Abdellah University, Faculty Of Science And Technology, Road Immouzer, BP 2202 Fez, Morocco, [c]Laboratory of Plant Chemistry, Organic and Bioorganic Synthesis, Faculty of Sciences, Mohammed V University in Rabat, 4 Avenue Ibn Battouta, BP 1014 RP, Morocco, [d]Science and Technology of Lille USR 3290, Villeneuve d'ascq cedex, France, [e]Department of Physics, Hacettepe University, 06800 Beytepe, Ankara, Türkiye, [f]Department of Chemistry, Tulane University, New Orleans, LA 70118, USA, [g]Laboratoire de Chimie Organique Appliquée, Université Sidi Mohamed Ben Abdallah, Faculté des Sciences et Techniques, Route dImmouzzer, BP 2202 Fez, Morocco, and [h]Laboratory of Organic and Physical Chemistry, Applied Bioorganic Chemistry Team, Faculty of Sciences, Ibn Zohr University, Agadir, Morocco. *Correspondence e-mail: mouad.lahyaoui@usmba.ac.ma

Received 25 October 2023
Accepted 15 November 2023

Edited by M. Weil, Vienna University of Technology, Austria

This article is part of a collection of articles to commemorate the founding of the African Crystallographic Association and the 75th anniversary of the IUCr.

Keywords: crystal structure; amino group; hydrogen bonding; heterocyclic compound.

CCDC reference: 2308262

Supporting information: this article has supporting information at journals.iucr.org/e

In the title molecule, $C_7H_7N_3O$, the pyrimidine ring is essentially planar, with the propynyl group rotated out of this plane by 15.31 (4)°. In the crystal, a tri-periodic network is formed by N—H···O, N—H···N and C—H···O hydrogen-bonding and slipped π–π stacking interactions, leading to narrow channels extending parallel to the *c* axis. Hirshfeld surface analysis of the crystal structure reveals that the most important contributions for the crystal packing are from H···H (36.2%), H···C/C···H (20.9%), H···O/O···H (17.8%) and H···N/N···H (12.2%) interactions, showing that hydrogen-bonding and van der Waals interactions are the dominant interactions in the crystal packing. Evaluation of the electrostatic, dispersion and total energy frameworks indicates that the stabilization is dominated by the electrostatic energy contributions. The molecular structure optimized by density functional theory (DFT) calculations at the B3LYP/6–311 G(d,p) level is compared with the experimentally determined structure in the solid state. The HOMO–LUMO behaviour was also elucidated to determine the energy gap.

1. Chemical context

Owing to their importance in the fields of pharmaceuticals, cytosine derivatives and their syntheses have been in the focus of chemists in recent years, in particular during the Covid pandemic period, for example with respect to the synthesis of Molnupiravir as an anti-viral drug (Sahoo & Subba Reddy, 2022). An alternative product identified as cytarabine, which also has been synthesized from cytosine, is a chemotherapy drug used to treat acute myeloid leukaemia (AML), acute lymphocytic leukaemia (ALL), chronic myeloid leukaemia (CML) and non-Hodgkin's lymphoma (Lamba, 2009; Güngör *et al.*, 2022). 1-(Prop-2-ynyl)-4-amino-2-oxopyrimidine was synthesized as an intermediate for the purpose of preparing other products that may have biological activities (Chatzileontiadou *et al.*, 2015).

In a continuation of our research work devoted to the study of N-alkylation reactions involving cytosine derivatives, we report herein on synthesis, molecular and crystal structures as well as Hirshfeld surface analysis, intermolecular interaction

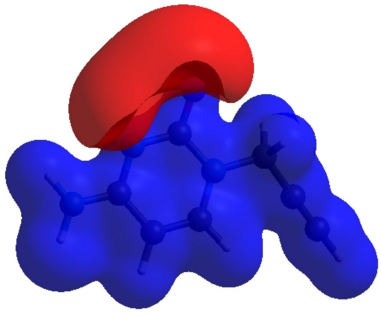

energies, energy frameworks and DFT-computational studies of the title compound (I), $C_7H_7N_3O$. This cytosine derivative was obtained by an alkylation reaction of cytosine using an excess of propargyl bromide as an alkylating reagent under the conditions of phase-transfer catalysis (PTC).

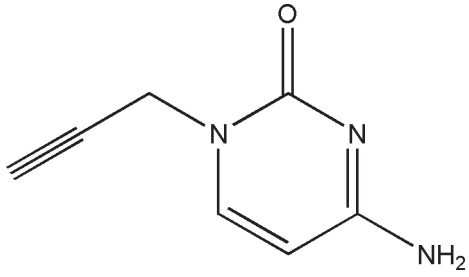

2. Structural commentary

The asymmetric unit of (I) comprises one molecule and is shown in Fig. 1. The pyrimidine ring is essentially planar (r.m.s.d = 0.0055 Å). The plane defined by the propynyl group (N1/C5/C6/C7) is inclined to the pyrimidine plane by 15.31 (4)°.

3. Supramolecular features

In the crystal, N3—H3*A*···O1 and C3—H3···O1 hydrogen bonds (Table 1) form chains of molecules extending along the *c*-axis direction. Inversion-related chains are connected by N3—H3*B*···N2 hydrogen bonds (Table 1), forming ribbons whose mean planes are inclined by ±31.4° to (010) (Fig. 2). The ribbons are linked by C7—H7···O1 hydrogen bonds (Table 1) and slipped π–π stacking interactions between pyrimidine rings [centroid-to-centroid distance = 3.6122 (6) Å, slippage = 1.51 Å] into the tri-periodic structure (Fig. 3), which has narrow channels running parallel to the *c* axis (Fig. 4).

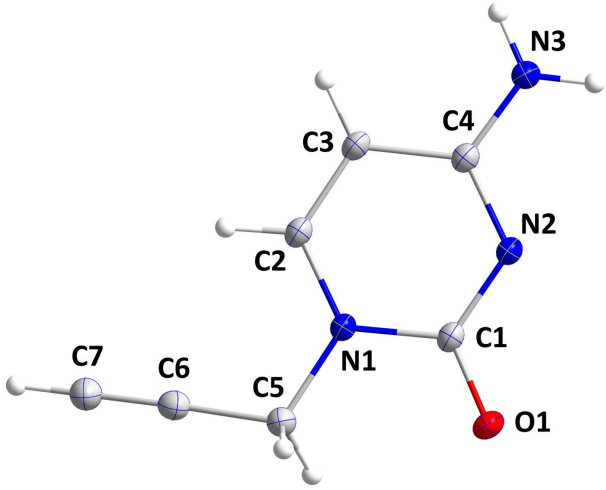

Figure 1
The title molecule with labelling scheme and displacement ellipsoids drawn at the 50% probability level.

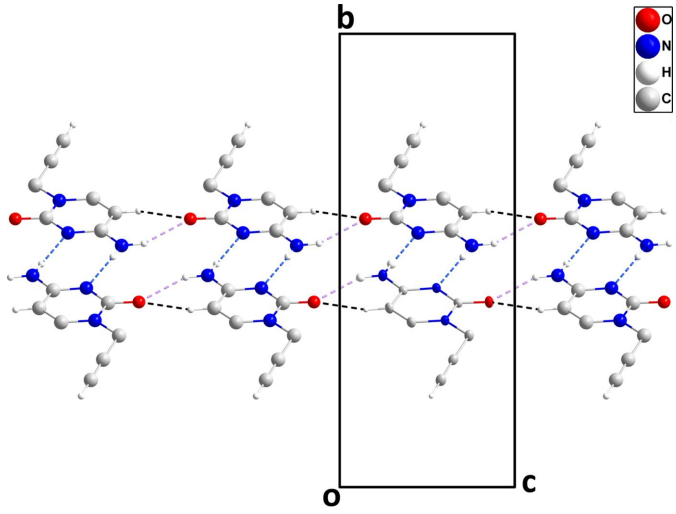

Figure 2
A portion of one ribbon viewed along the *a* axis with N—H···N, N—H···O and C—H···O hydrogen bonds depicted, respectively, by blue, violet and black dashed lines.

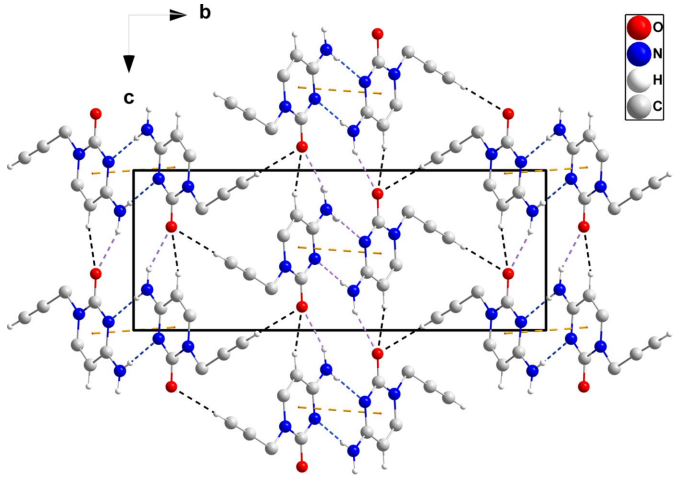

Figure 3
Packing of (I) viewed along the *a* axis with hydrogen bonds depicted as in Fig. 2. The π–π stacking interactions are depicted by orange dashed lines.

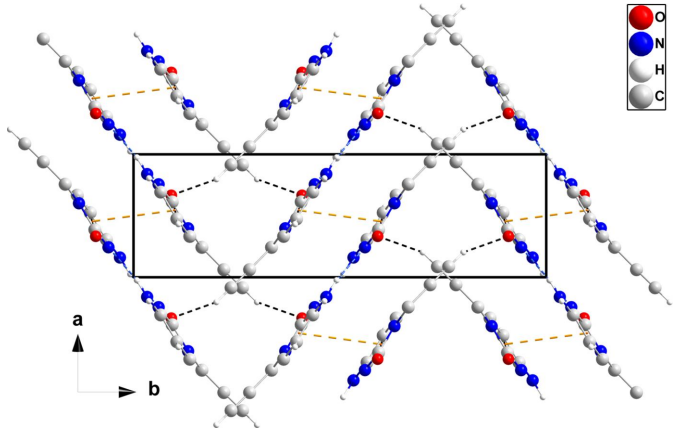

Figure 4
Packing viewed along the *c* axis with hydrogen bonds depicted as in Fig. 2, and with π–π stacking interactions as in Fig. 3.

Table 1
Hydrogen-bond geometry (Å, °).

D—H···A	D—H	H···A	D···A	D—H···A
N3—H3A···O1^{i}	0.89 (1)	2.16 (1)	3.0002 (9)	156 (1)
N3—H3B···N2^{ii}	0.90 (1)	2.10 (1)	2.9854 (10)	169 (1)
C3—H3···O1^{i}	0.95	2.56	3.3036 (10)	135
C7—H7···O1^{iii}	0.95	2.37	3.2559 (11)	156

Symmetry codes: (i) $x, y, z-1$; (ii) $-x+2, -y+1, -z+1$; (iii) $x-1, -y+\frac{1}{2}, z-\frac{1}{2}$.

4. Hirshfeld surface analysis

In order to visualize the intermolecular interactions in the crystal of (I), a Hirshfeld surface (HS) analysis (Hirshfeld, 1977; Spackman & Jayatilaka, 2009) was carried out by using *CrystalExplorer* (Spackman *et al.*, 2021). In the HS plotted over d_{norm} (Fig. 5), the white surface indicates contacts with distances equal to the sum of the van der Waals radii, and the red and blue colours indicate distances shorter (in close contact) or longer (distinct contacts) than the van der Waals radii, respectively (Venkatesan *et al.*, 2016). The bright-red spots appearing near O1, N2 and hydrogen atom H3*A* indicate their roles as the respective donors and/or acceptors atoms for hydrogen bonding; they also appear as blue and red regions corresponding to positive and negative potentials on the HS mapped over electrostatic potential (Spackman *et al.*, 2008; Jayatilaka *et al.*, 2005) shown in Fig. 6. The blue regions indicate positive electrostatic potential (hydrogen-bond donors), while the red regions indicate negative electrostatic potential (hydrogen-bond acceptors). The shape-index of the HS is a tool to visualize π–π stacking interactions by the presence of adjacent red and blue triangles (Fig. 7). The overall two-dimensional fingerprint plot, Fig. 8*a*, and those delineated into H···H, H···C/C···H, H···O/O···H, H···N/N···H, C···C, C···N/N···C, N···N, C···O/O···C and N···O/O···N (McKinnon *et al.*, 2007) are illustrated in Fig. 8*b*–*j*, together with their relative contributions to the Hirshfeld surface. The most important interaction originates from H···H contacts, contributing 36.2% to the overall crystal packing, which is reflected in Fig. 8*b* as widely scattered points

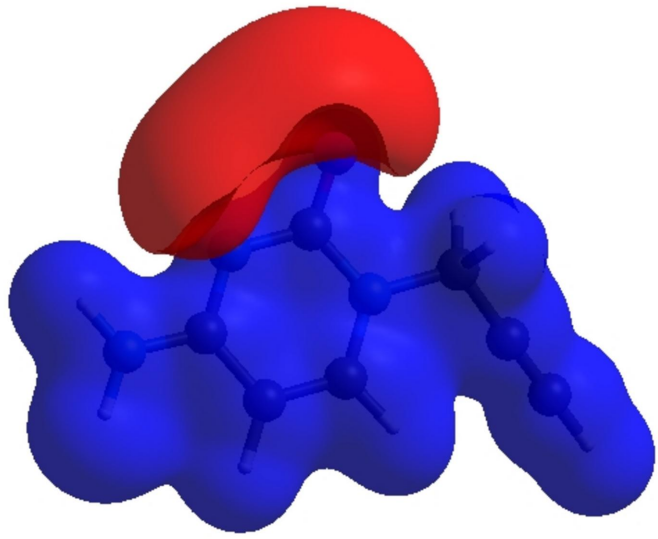

Figure 6
View of the three-dimensional Hirshfeld surface of the title compound plotted over electrostatic potential energy in the range −0.0500 to 0.0500 a.u. using the STO-3 G basis set at the Hartree–Fock level of theory. Hydrogen-bond donors and acceptors are shown as blue and red regions around the atoms, corresponding to positive and negative potentials, respectively.

of high density due to the large hydrogen content of the molecule with the tip at $d_e = d_i = 1.20$ Å. In the absence of C—H···π interactions, the H···C/C···H contacts, contributing 20.9% to the overall crystal packing, are shown in Fig. 8*c* with the tips at $d_e + d_i = 2.57$ Å. The pair of characteristic wings in the fingerprint plot delineated into H···O/O···H contacts (Fig. 8*d*) with a 17.8% contribution to the HS is viewed as a pair of spikes with the tips at $d_e + d_i = 2.05$ Å. The pair of characteristic wings in the fingerprint plot delineated into H···N/N···H contacts (Fig. 8*e*, 12.2% contribution to the HS) is viewed as a pair of spikes with the tips at $d_e + d_i = 2.00$ Å. The C···C contacts, contributing with 6.1% to the

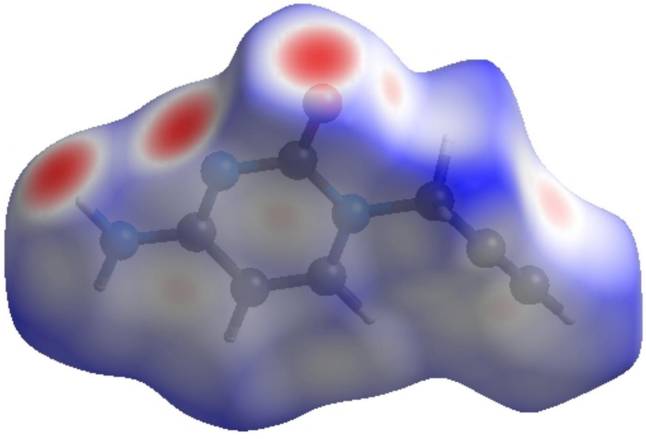

Figure 5
View of the three-dimensional Hirshfeld surface of the title compound plotted over d_{norm} in the range of −0.4969 to 1.1244 a.u.

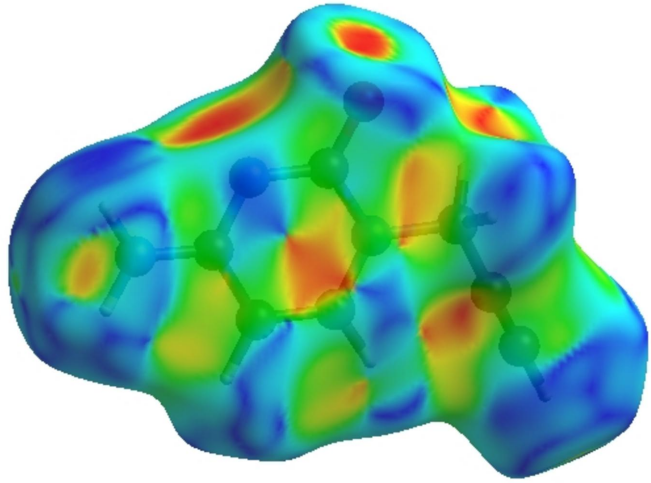

Figure 7
Hirshfeld surface of the title compound plotted over shape-index.

Table 3
Calculated energies and quantum-chemical parameters of (I).

Total Energy, *TE* (eV)	−13800.94
E_{HOMO} (eV)	−9.28
E_{LUMO} (eV)	−2.64
Gap, ΔE (eV)	6.64
Dipole moment, μ (Debye)	7.47
Ionization potential, I (eV)	9.28
Electron affinity, A	2.64
Electronegativity, χ	3.20
Hardness, η	5.96
Softness, σ	0.15
Electrophilicity index, ω	5.35

overall crystal packing, have a bullet-shaped distribution of points. They are shown in Fig. 8*f* with the tip at $d_e = d_i$ = 1.61 Å. The C···N/N···C contacts,which contribute 5.1% to the overall crystal packing, have a bat-shaped distribution of points (Fig. 8*g*) with the tips at $d_e + d_i$ = 3.28 Å. Finally, the N···N (Fig. 8*h*), C···O/O···C (Fig. 8*i*) and N···O/O···N (Fig. 8*j*) contacts contribute 0.9%, 0.4% and 0.3%, respectively, to the HS. The functions d_{norm} plotted onto the HS are

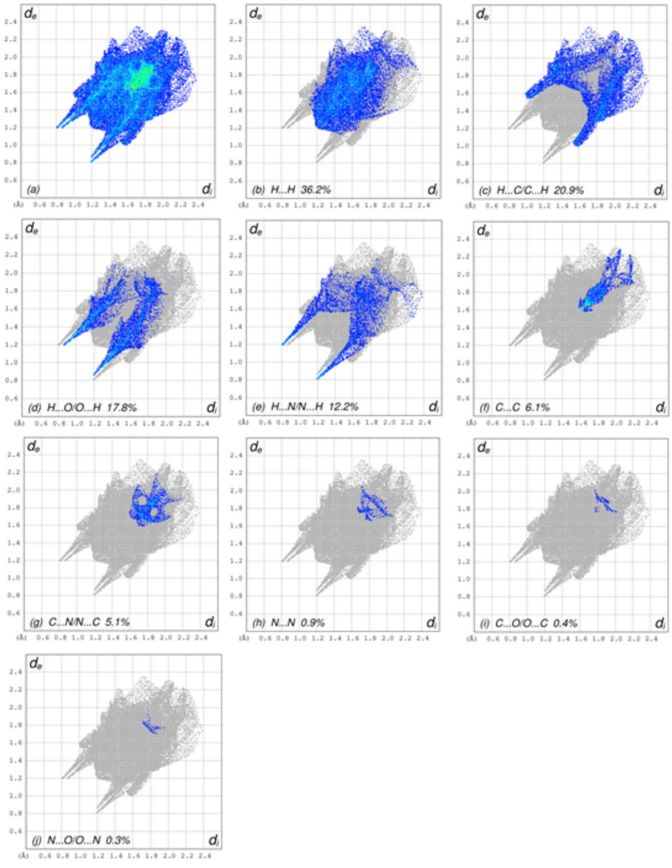

Figure 8
The full two-dimensional fingerprint plots for the title compound, showing (*a*) all interactions, and delineated into (*b*) H···H, (*c*) H···C/C···H, (*d*) H···O/O···H, (*e*) H···N/ N···H, (*f*) C···C, (*g*) C···N/N···C, (*h*) N···N, (i) C···O/O···C and (*j*) N···O/O···N interactions. The d_i and d_e values are the closest internal and external distances (in Å) from given points on the Hirshfeld surface.

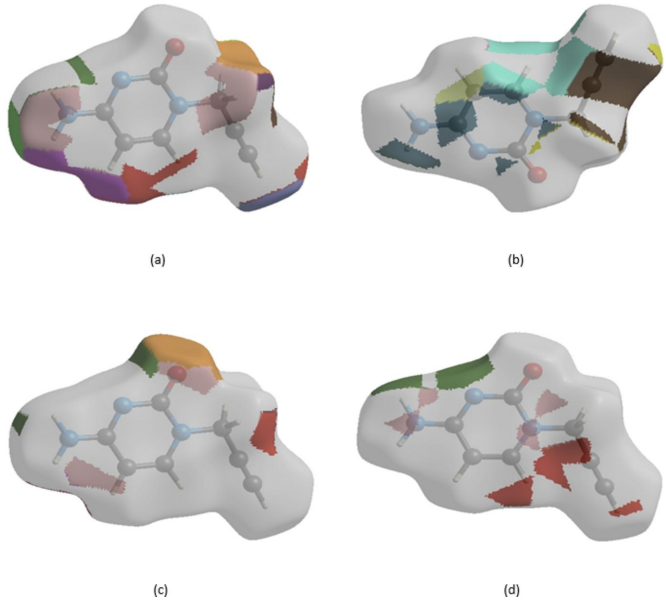

Figure 9
The Hirshfeld surface representations with the function d_{norm} plotted onto the surface for (*a*) H···H, (*b*) H···C/C···H, (*c*) H···O/O···H and (*d*) H···N/N···H interactions.

shown for the H···H, H···C/C···H, H···O/O···H and H···N/N···H interactions in Fig. 9*a–d*. The HS analysis confirms the importance of H-atom contacts in establishing the packing and suggest that van der Waals interactions and hydrogen-bonding play the major roles in the crystal packing (Hathwar *et al.*, 2015).

5. Interaction energy calculations and energy frameworks

The intermolecular interaction energies were calculated using the CE–B3LYP/6–31G(d,p) energy model available in *CrystalExplorer* (Spackman *et al.*, 2021), where a cluster of molecules is generated by applying crystallographic symmetry operations with respect to a selected central molecule within the radius of 3.8 Å by default (Turner *et al.*, 2014). The total intermolecular energy (E_{tot}) is the sum of electrostatic (E_{ele}), polarization (E_{pol}), dispersion (E_{dis}) and exchange-repulsion (E_{rep}) energies (Turner *et al.*, 2015) with scale factors of 1.057, 0.740, 0.871 and 0.618, respectively (Mackenzie *et al.*, 2017). Energy frameworks combine the calculation of intermolecular interaction energies with a graphical representation of their magnitude (Turner *et al.*, 2015). Energies between molecular pairs are represented as cylinders joining the centroids of pairs of molecules with the cylinder radius proportional to the relative strength of the corresponding interaction energy. Energy frameworks were constructed for E_{ele} (red cylinders), E_{dis} (green cylinders) and E_{tot} (blue cylinders) and are shown in Fig. 10*a–c*. The evaluation of the electrostatic, dispersion and total energy frameworks reveals that the stabilization is dominated by the electrostatic energy contribution in the crystal structure of (I).

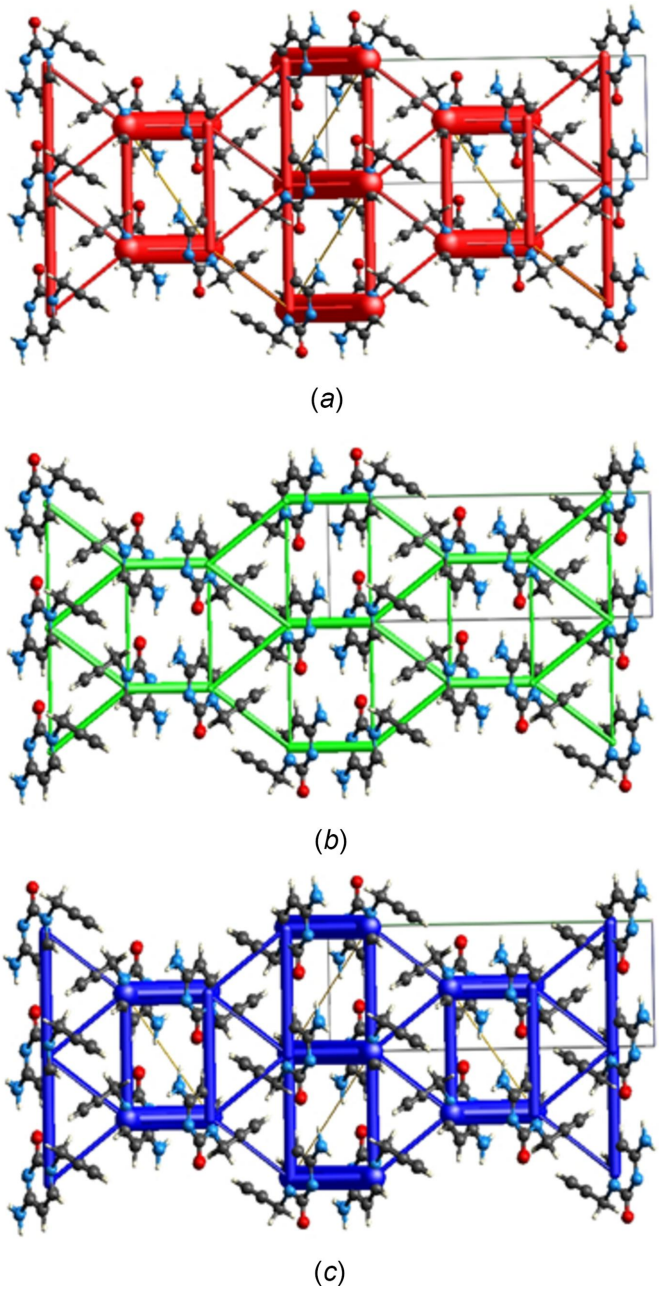

Figure 10
The views of the energy frameworks for a cluster of molecules of the title compound showing (*a*) electrostatic energy, (*b*) dispersion energy and (*c*) total energy diagrams. The cylinder radii are proportional to the relative strength of the corresponding energies, adjusted to the same scale factor of 80 with a cut-off value of 5 kJ mol^{-1} within 2×2×2 unit cells.

6. DFT calculations

Bond lengths and angles as well as energies of (I) in the gas phase were computed on basis of density functional theory (DFT) using the standard B3LYP functional and the 6–311G(d,p) basis-set (Becke, 1993) as implemented in *GAUSSIAN 09* (Frisch *et al.*, 2009). Table 2 reveals that the calculated bond lengths and angles are in good agreement with the experimentally determined values. The HOMO-LUMO energy gap of the molecule was also calculated by the DFT/B3LYP/6-311G(d,p) method and is shown in Fig. 11. Furthermore, quantum chemistry descriptors (chemical hardness η, softness S, electronegativity χ and electrophilicity w) derived from the conceptual DFT calculations of (I) are given in Table 3. The HOMO and LUMO are localized in the plane extending from the whole 4-amino-1-(prop-2-yn-1-yl)pyrimidin-2(1*H*)-one ring. The energy band gap [$\Delta E = E_{LUMO} - E_{HOMO}$] of the molecule is 6.64 eV, and the frontier molecular orbital energies, E_{HOMO} and E_{LUMO} are −9.28 eV and −2.64 eV, respectively.

Table 2
Comparison of selected X-ray and DFT bond lengths and angles (Å, °).

Bonds/angles	X-ray	B3LYP/6–311G(d,p)
O1—C1	1.2444 (9)	1.2457
N1—C2	1.3632 (10)	1.3645
N1—C5	1.4716 (10)	1.4782
N2—C4	1.3415 (10)	1.3423
N2—C1	1.3570 (10)	1.3542
N3—C4	1.3353 (10)	1.3392
C2—N1—C1	120.71 (6)	120.82
O1—C1—N2	122.47 (7)	122.17
O1—C1—N1	118.64 (7)	118.54
N2—C1—N1	118.88 (6)	118.53

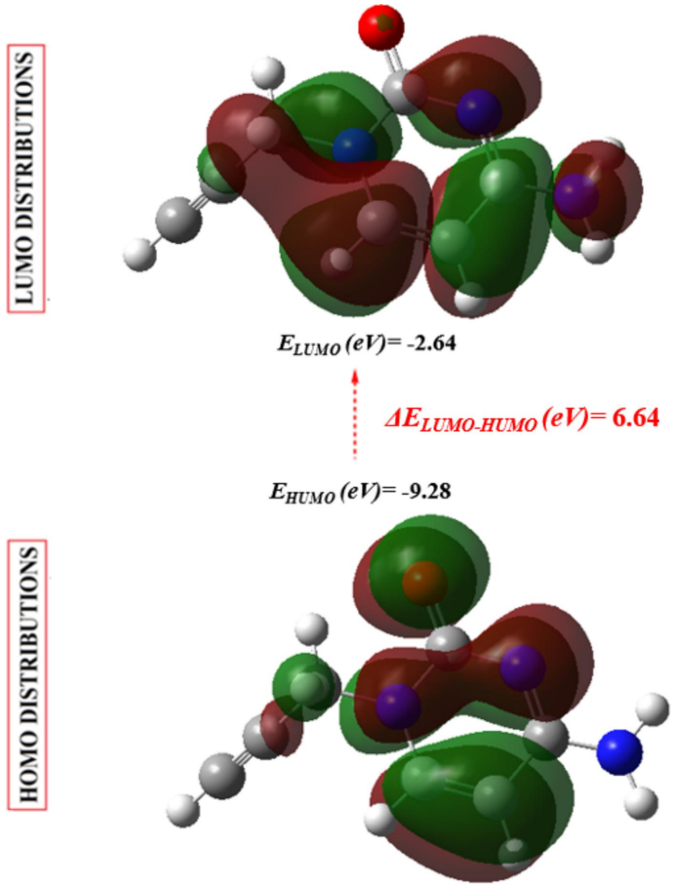

Figure 11
The energy band gap of (I).

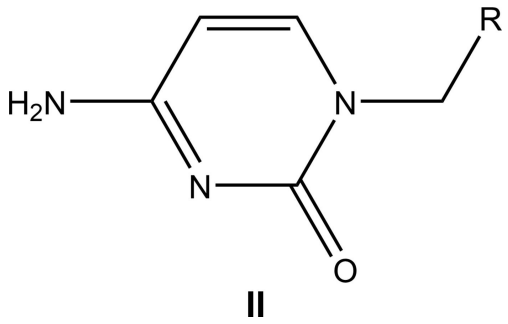

II

Figure 12
The molecular fragment **II** used for the database search.

7. Database survey

A search of the Cambridge Structural Database (CSD, version 5.42, current as of October 2023; Groom *et al.*, 2016) with the search fragment **II** (Fig. 12) generated 37 hits also including co-crystals, metal complexes and ions protonated on the doubly bonded nitrogen atom. The most comparable structures to (I) include those with R = $CH_2CO_2Bu^i$ (COFJIS; Geng *et al.*, 2013), 2-oxido-2-phenoxy-1,4,2-dioxaphosphinan-5-yl (DATZIJ; Krylov *et al.*, 2012), $CH_2C(=O)NHC(COOH)CH_2(4\text{-}OHC_6H_4)$ (COQNAX; Doi *et al.*, 1999), $(CH_2)_3SiMe_2Ph$ (HIXKOQ; Kociok-Köhn *et al.*, 2014), $CH{=}CHCH_2NHC(=O)(4\text{-}FC_6H_4)$ (PEYHOS; Cetina *et al.*, 2012), CH_2OH (DECYUF; Shibata *et al.*, 1985), $CH_2C(=O)NH_2$ (CIMJEN; Fujita *et al.*, 1984), $CH_2C(=O)NHC(COO^-)(CH_2)_4NH_3^+$ (LAVZEO; Doi *et al.*, 2005), 2′-deoxy-β-D-ribo-pentofuranosyl (NAGLIQ; Hossain *et al.*, 1996), 4-pyridyl (KUDPEH; Tufenkjian *et al.*, 2020), $CH{=}CHCH_2NHC(O)Ph$ (PEHYEI; Cetina *et al.*, 2012) and *n*-pentyl (YINGAF; Barceló-Oliver *et al.*, 2013). In all of these structures, the first two atoms of the substituent are rotated by nearly 90° from being coplanar with the pyrimidine ring, in contrast to what is observed for (I). In all cases this is likely due to steric hindrance between hydrogen atoms on the substituent and the adjacent ring hydrogen and the carbonyl oxygen. However, in COQNAX there is a possible, weak π-stacking interaction that could also direct the conformation. In NAGLIQ, there is a weak C—H$\cdots\pi$(ring) interaction that could act similarly.

8. Synthesis and crystallization

A mixture of cytosine (1.5 mmol) and potassium carbonate (K_2CO_3) (3 mmol) was dissolved in 25 ml of dimethylformamide (DMF). The solution was stirred magnetically for 10 min., followed by addition of 0.01 equivalents of tetra-*n*-butylammonium bromide (TBAB) and 3 mmol of propargyl bromide. The mixture was stirred magnetically for 24 h. After filtration of the formed salts, the DMF was evaporated under reduced pressure. The residue obtained was purified by chromatography on a silica gel column. Single crystals of (I) suitable for X-ray diffraction were obtained by slow evaporation of an ethanol solution. ^{1}H NMR (300 MHz, DMSO-d_6): 3.306–3.322 (*t*, 1H, CH≡C, J = 2.4, 4.8); 4.482–4.49 (*d*, 2H, CH_2, J = 2.4); 5.806–5.83 (*d*, 1H, CH, J = 7.2); 7.109 (*s*, 1H, NH); 7.37 (*s*, 1H, NH); 7.669–7.693 (*d*, 1H, CH—N, J = 7.2). ^{13}C NMR (75 MHz, DMSO): 37.95 (CH_2); 75.78 (C≡CH); 94.93 (CH≡C); 141.48 (CH—N); 143.24 (CH—C); 156.05 (C═O); 166.42 (C═N).

Table 4
Experimental details.

Crystal data	
Chemical formula	$C_7H_7N_3O$
M_r	149.16
Crystal system, space group	Monoclinic, $P2_1/c$
Temperature (K)	150
a, b, c (Å)	5.3864 (6), 18.013 (2), 7.0112 (8)
β (°)	96.288 (4)
V (Å^3)	676.18 (13)
Z	4
Radiation type	Mo $K\alpha$
μ (mm^{-1})	0.10
Crystal size (mm)	0.34 × 0.32 × 0.07
Data collection	
Diffractometer	Bruker D8 QUEST PHOTON 3 diffractometer
Absorption correction	Numerical (*SADABS*; Krause *et al.*, 2015)
T_{min}, T_{max}	0.96, 0.99
No. of measured, independent and observed [$I > 2\sigma(I)$] reflections	28024, 2554, 2251
R_{int}	0.035
(sin $\theta/\lambda)_{max}$ (Å^{-1})	0.770
Refinement	
$R[F^2 > 2\sigma(F^2)]$, $wR(F^2)$, S	0.040, 0.113, 1.05
No. of reflections	2554
No. of parameters	108
No. of restraints	2
H-atom treatment	H atoms treated by a mixture of independent and constrained refinement
$\Delta\rho_{max}$, $\Delta\rho_{min}$ (e Å^{-3})	0.47, −0.20

Computer programs: *APEX3* and *SAINT* (Bruker, 2020), *SHELXT* (Sheldrick, 2015*a*), *SHELXL* (Sheldrick, 2015*b*), *DIAMOND* (Brandenburg & Putz, 2012) and *publCIF* (Westrip, 2010).

9. Refinement

Crystal data, data collection and structure refinement details are summarized in Table 4. H atoms attached to carbon atoms were placed in idealized positions and were included as riding contributions with isotropic displacement parameters 1.2–1.5 times those of the parent atoms. Those attached to nitrogen were placed in locations derived from a difference-Fourier map and refined with a distance of 0.90 (1) Å. Reflection 020 was affected by the beamstop and was omitted from the final refinement.

Funding information

JTM thanks Tulane University for support of the Tulane Crystallography Laboratory. TH is grateful to Hacettepe University Scientific Research Project Unit (grant No. 013 D04 602 004).

References

Barceló-Oliver, M., Bauzá, A., Baquero, B. A., García-Raso, A., Terrón, A., Molins, E. & Frontera, A. (2013). *Tetrahedron Lett.* **54**, 5355–5360.

Becke, A. D. (1993). *J. Chem. Phys.* **98**, 5648–5652.

Brandenburg, K. & Putz, H. (2012). *DIAMOND*, Crystal Impact GbR, Bonn, Germany.

Bruker (2020). *APEX3* and *SAINT*. Bruker AXS LLC, Madison, Wisconsin, USA.

Cetina, M., Benci, K., Wittine, K. & Mintas, M. (2012). *Cryst. Growth Des.* **12**, 5262–5270.

Chatzileontiadou, D. S., Parmenopoulou, V., Manta, S., Kantsadi, A. L., Kylindri, P., Griniezaki, M., Kontopoulou, F., Telopoulou, A., Prokova, H., Panagopoulos, D., Boix, E., Balatsos, N. A. A., Komiotis, D. & Leonidas, D. D. (2015). *Bioorg. Chem.* **63**, 152–165.

Doi, M., Miyako, H., Asano, A. & Ishida, T. (1999). *Anal. Sci.* **15**, 109–110.

Doi, M., Nakamoto, Y. & Asano, A. (2005). *Acta Cryst.* C**61**, o577–o582.

Frisch, M. J., Trucks, G. W., Schlegel, H. B., Scuseria, G. E., Robb, M. A., Cheeseman, J. R., Scalmani, G., Barone, V., Mennucci, B., Petersson, G. A., Nakatsuji, H., Caricato, M., Li, X., Hratchian, H. P., Izmaylov, A. F., Bloino, J., Zheng, G., Sonnenberg, J. L., Hada, M., Ehara, M., Toyota, K., Fukuda, R., Hasegawa, J., Ishida, M., Nakajima, T., Honda, Y., Kitao, O., Nakai, H., Vreven, T., Montgomery, J. A. Jr, Peralta, J. E., Ogliaro, F., Bearpark, M., Heyd, J. J., Brothers, E., Kudin, K. N., Staroverov, V. N., Kobayashi, R., Normand, J., Raghavachari, K., Rendell, A., Burant, J. C., Iyengar, S. S., Tomasi, J., Cossi, M., Rega, N., Millam, J. M., Klene, M., Knox, J. E., Cross, J. B., Bakken, V., Adamo, C., Jaramillo, J., Gomperts, R., Stratmann, R. E., Yazyev, O., Austin, A. J., Cammi, R., Pomelli, C., Ochterski, J. W., Martin, R. L., Morokuma, K., Zakrzewski, V. G., Voth, G. A., Salvador, P., Dannenberg, J. J., Dapprich, S., Daniels, A. D., Farkas, O., Foresman, J. B., Ortiz, J. V., Cioslowski, J. & Fox, D. J. (2009). *GAUSSIAN09*. Gaussian Inc., Wallingford, CT, US

Fujita, S., Takenaka, A. & Sasada, Y. (1984). *Acta Cryst.* C**40**, 1467–1469.

Geng, L.-L., Wang, C., Yuan, W. & Song, X.-M. (2013). *Z. Krist. New Cryst. Struct.* **228**, 447–448.

Groom, C. R., Bruno, I. J., Lightfoot, M. P. & Ward, S. C. (2016). *Acta Cryst.* B**72**, 171–179.

Güngör, Ö., Demircioğlu, Z. & Gölcü, A. (2022). *J. Mol. Struct.* **1270**, 133826.

Hathwar, V. R., Sist, M., Jørgensen, M. R. V., Mamakhel, A. H., Wang, X., Hoffmann, C. M., Sugimoto, K., Overgaard, J. & Iversen, B. B. (2015). *IUCrJ*, **2**, 563–574.

Hirshfeld, H. L. (1977). *Theor. Chim. Acta*, **44**, 129–138.

Hossain, N., Blaton, N., Peeters, O., Rozenski, J. & Herdewijn, P. A. (1996). *Tetrahedron*, **52**, 5563–5578.

Jayatilaka, D., Grimwood, D. J., Lee, A., Lemay, A., Russel, A. J., Taylor, C., Wolff, S. K., Cassam-Chenai, P. & Whitton, A. (2005). *TONTO - A System for Computational Chemistry. Available at*: http://hirshfeldsurface.net/

Kociok-Köhn, G., Mahon, M. F., Molloy, K. C., Price, G. J., Prior, T. J. & Smith, D. R. G. (2014). *Dalton Trans.* **43**, 7734–7746.

Krause, L., Herbst-Irmer, R., Sheldrick, G. M. & Stalke, D. (2015). *J. Appl. Cryst.* **48**, 3–10.

Krylov, I. S., Zakharova, V. M., Serpi, M., Haiges, R., Kashemirov, B. A. & McKenna, C. E. (2012). *J. Org. Chem.* **77**, 684–689.

Lamba, J. K. (2009). *Pharmacogenomics*, **10**, 1657–1674.

Mackenzie, C. F., Spackman, P. R., Jayatilaka, D. & Spackman, M. A. (2017). *IUCrJ*, **4**, 575–587.

McKinnon, J. J., Jayatilaka, D. & Spackman, M. A. (2007). *Chem. Commun.* pp. 3814–3816.

Sahoo, T. & Subba Reddy, B. V. (2022). *Tetrahedron Lett.* **97**, 153783.

Sheldrick, G. M. (2015*a*). *Acta Cryst.* A**71**, 3–8.

Sheldrick, G. M. (2015*b*). *Acta Cryst.* C**71**, 3–8.

Shibata, M., Takenaka, A., Sasada, Y. & Ohki, M. (1985). *Acta Cryst.* C**41**, 1354–1356.

Spackman, M. A. & Jayatilaka, D. (2009). *CrystEngComm*, **11**, 19–32.

Spackman, M. A., McKinnon, J. J. & Jayatilaka, D. (2008). *CrystEngComm*, **10**, 377–388.

Spackman, P. R., Turner, M. J., McKinnon, J. J., Wolff, S. K., Grimwood, D. J., Jayatilaka, D. & Spackman, M. A. (2021). *J. Appl. Cryst.* **54**, 1006–1011.

Tufenkjian, E., Jouaiti, A., Kyritsakas, N., Hosseini, M. W. & Bulach, V. (2020). *Tetrahedron*, **76**, 130966.

Turner, M. J., Grabowsky, S., Jayatilaka, D. & Spackman, M. A. (2014). *J. Phys. Chem. Lett.* **5**, 4249–4255.

Turner, M. J., Thomas, S. P., Shi, M. W., Jayatilaka, D. & Spackman, M. A. (2015). *Chem. Commun.* **51**, 3735–3738.

Venkatesan, P., Thamotharan, S., Ilangovan, A., Liang, H. & Sundius, T. (2016). *Spectrochim. Acta A Mol. Biomol. Spectrosc.* **153**, 625–636.

Westrip, S. P. (2010). *J. Appl. Cryst.* **43**, 920–925.

supporting information

Acta Cryst. (2023). E**79**, 1183-1189 [https://doi.org/10.1107/S2056989023009933]

Crystal structure, Hirshfeld surface analysis, intermolecular interaction energies, energy frameworks and DFT calculations of 4-amino-1-(prop-2-yn-1-yl)pyrimidin-2(1*H*)-one

Mouad Lahyaoui, Amal Haoudi, Badr Eddine Kartah, Ahmed Mazzah, Tuncer Hökelek, Joel T. Mague, Youssef Kandri Rodi and Nada Kheira Sebbar

Computing details

4-Amino-1-(prop-2-yn-1-yl)pyrimidin-2(1*H*)-one

Crystal data

$C_7H_7N_3O$
M_r = 149.16
Monoclinic, $P2_1/c$
a = 5.3864 (6) Å
b = 18.013 (2) Å
c = 7.0112 (8) Å
β = 96.288 (4)°
V = 676.18 (13) Å^3
Z = 4
$F(000)$ = 312
D_x = 1.465 Mg m^{-3}
Mo $K\alpha$ radiation, λ = 0.71073 Å
Cell parameters from 9914 reflections
θ = 4.0–33.2°
μ = 0.10 mm^{-1}
T = 150 K
Plate, colourless
0.34 × 0.32 × 0.07 mm

Data collection

Bruker D8 QUEST PHOTON 3 diffractometer
Radiation source: fine-focus sealed tube
Graphite monochromator
Detector resolution: 7.3910 pixels mm^{-1}
ω scans
Absorption correction: numerical (*SADABS*; Krause *et al.*, 2015)
T_{min} = 0.96, T_{max} = 0.99
28024 measured reflections
2554 independent reflections
2251 reflections with $I > 2\sigma(I)$
R_{int} = 0.035
θ_{max} = 33.2°, θ_{min} = 4.0°
h = −8→8
k = −27→27
l = −10→10

Refinement

Refinement on F^2
Least-squares matrix: full
$R[F^2 > 2\sigma(F^2)]$ = 0.040
$wR(F^2)$ = 0.113
S = 1.05
2554 reflections
108 parameters
2 restraints
Primary atom site location: dual
Secondary atom site location: difference Fourier map
Hydrogen site location: mixed
H atoms treated by a mixture of independent and constrained refinement
$w = 1/[\sigma^2(F_o^2) + (0.0627P)^2 + 0.1628P]$ where $P = (F_o^2 + 2F_c^2)/3$
$(\Delta/\sigma)_{max} < 0.001$
$\Delta\rho_{max}$ = 0.47 e Å^{-3}
$\Delta\rho_{min}$ = −0.20 e Å^{-3}

Special details

Experimental. The diffraction data were obtained from 8 sets of frames, each of width 0.5° in ω, collected with scan parameters determined by the "strategy" routine in *APEX3*. The scan time was 5 sec/frame.

Geometry. All esds (except the esd in the dihedral angle between two l.s. planes) are estimated using the full covariance matrix. The cell esds are taken into account individually in the estimation of esds in distances, angles and torsion angles; correlations between esds in cell parameters are only used when they are defined by crystal symmetry. An approximate (isotropic) treatment of cell esds is used for estimating esds involving l.s. planes.

Refinement. Refinement of F^2 against ALL reflections. The weighted R-factor wR and goodness of fit S are based on F^2, conventional R-factors R are based on F, with F set to zero for negative F^2. The threshold expression of $F^2 > 2\text{sigma}(F^2)$ is used only for calculating R-factors(gt) etc. and is not relevant to the choice of reflections for refinement. R-factors based on F^2 are statistically about twice as large as those based on F, and R- factors based on ALL data will be even larger. H-atoms attached to carbon were placed in calculated positions (C—H = 0.95 - 1.00 Å) and were included as riding contributions with isotropic displacement parameters 1.2 - 1.5 times those of the attached atoms. Those attached to nitrogen were placed in locations derived from a difference map and refined with a DFIX 0.91 0.01 instruction. One reflection affected by the beamstop was omitted from the final refinement.

Fractional atomic coordinates and isotropic or equivalent isotropic displacement parameters (Å²)

	x	*y*	*z*	U_{iso}*/U_{eq}
O1	0.66696 (11)	0.40841 (3)	0.85317 (8)	0.01939 (14)
N1	0.39821 (12)	0.36777 (4)	0.60167 (9)	0.01532 (14)
N2	0.75623 (12)	0.43923 (3)	0.55258 (9)	0.01525 (14)
N3	0.83960 (13)	0.46704 (4)	0.24590 (10)	0.01878 (15)
H3A	0.805 (3)	0.4626 (8)	0.1187 (12)	0.031 (3)*
H3B	0.976 (2)	0.4921 (7)	0.296 (2)	0.033 (3)*
C1	0.61327 (14)	0.40625 (4)	0.67606 (11)	0.01469 (14)
C2	0.33252 (14)	0.36368 (4)	0.40859 (11)	0.01677 (15)
H2	0.183831	0.338315	0.361154	0.020*
C3	0.47496 (14)	0.39504 (4)	0.28349 (11)	0.01730 (15)
H3	0.431950	0.391252	0.148775	0.021*
C4	0.69319 (14)	0.43416 (4)	0.36256 (11)	0.01446 (14)
C5	0.24325 (15)	0.33434 (4)	0.73922 (11)	0.01883 (16)
H5A	0.352977	0.308719	0.841101	0.023*
H5B	0.153456	0.374207	0.800556	0.023*
C6	0.06137 (15)	0.28125 (4)	0.64860 (11)	0.01895 (16)
C7	−0.08594 (16)	0.23629 (5)	0.57853 (12)	0.02220 (17)
H7	−0.202500	0.200721	0.523077	0.027*

Atomic displacement parameters (Å²)

	U^{11}	U^{22}	U^{33}	U^{12}	U^{13}	U^{23}
O1	0.0215 (3)	0.0237 (3)	0.0123 (3)	−0.0033 (2)	−0.0012 (2)	−0.00096 (19)
N1	0.0150 (3)	0.0178 (3)	0.0128 (3)	−0.0033 (2)	0.0001 (2)	−0.0006 (2)
N2	0.0154 (3)	0.0169 (3)	0.0130 (3)	−0.0025 (2)	−0.0001 (2)	−0.0009 (2)
N3	0.0190 (3)	0.0232 (3)	0.0140 (3)	−0.0051 (2)	0.0011 (2)	0.0000 (2)
C1	0.0142 (3)	0.0153 (3)	0.0140 (3)	−0.0008 (2)	−0.0008 (2)	−0.0015 (2)
C2	0.0161 (3)	0.0194 (3)	0.0142 (3)	−0.0028 (2)	−0.0009 (2)	−0.0017 (2)
C3	0.0177 (3)	0.0207 (3)	0.0130 (3)	−0.0034 (2)	−0.0008 (2)	−0.0023 (2)
C4	0.0145 (3)	0.0148 (3)	0.0138 (3)	0.0002 (2)	0.0003 (2)	−0.0010 (2)

C5	0.0195 (3)	0.0218 (3)	0.0151 (3)	−0.0051 (3)	0.0014 (3)	0.0004 (2)
C6	0.0192 (3)	0.0206 (3)	0.0170 (3)	−0.0014 (3)	0.0019 (3)	0.0025 (3)
C7	0.0227 (4)	0.0240 (4)	0.0195 (4)	−0.0044 (3)	0.0007 (3)	0.0015 (3)

Geometric parameters (Å, º)

O1—C1	1.2444 (9)	C2—C3	1.3507 (11)
N1—C2	1.3632 (10)	C2—H2	0.9500
N1—C1	1.4007 (10)	C3—C4	1.4294 (10)
N1—C5	1.4716 (10)	C3—H3	0.9500
N2—C4	1.3415 (10)	C5—C6	1.4635 (11)
N2—C1	1.3570 (10)	C5—H5A	0.9900
N3—C4	1.3353 (10)	C5—H5B	0.9900
N3—H3A	0.894 (8)	C6—C7	1.2005 (11)
N3—H3B	0.899 (9)	C7—H7	0.9500
C2—N1—C1	120.71 (6)	C2—C3—H3	121.4
C2—N1—C5	121.63 (6)	C4—C3—H3	121.4
C1—N1—C5	117.63 (6)	N3—C4—N2	118.42 (7)
C4—N2—C1	120.28 (6)	N3—C4—C3	119.79 (7)
C4—N3—H3A	120.0 (9)	N2—C4—C3	121.78 (7)
C4—N3—H3B	119.5 (10)	C6—C5—N1	112.56 (6)
H3A—N3—H3B	120.4 (13)	C6—C5—H5A	109.1
O1—C1—N2	122.47 (7)	N1—C5—H5A	109.1
O1—C1—N1	118.64 (7)	C6—C5—H5B	109.1
N2—C1—N1	118.88 (6)	N1—C5—H5B	109.1
C3—C2—N1	121.21 (7)	H5A—C5—H5B	107.8
C3—C2—H2	119.4	C7—C6—C5	178.11 (9)
N1—C2—H2	119.4	C6—C7—H7	180.0
C2—C3—C4	117.12 (7)		
C4—N2—C1—O1	178.71 (7)	N1—C2—C3—C4	−1.57 (11)
C4—N2—C1—N1	−0.74 (10)	C1—N2—C4—N3	−179.62 (7)
C2—N1—C1—O1	−179.75 (7)	C1—N2—C4—C3	0.61 (11)
C5—N1—C1—O1	2.17 (10)	C2—C3—C4—N3	−179.22 (7)
C2—N1—C1—N2	−0.27 (11)	C2—C3—C4—N2	0.55 (11)
C5—N1—C1—N2	−178.35 (6)	C2—N1—C5—C6	15.87 (11)
C1—N1—C2—C3	1.48 (12)	C1—N1—C5—C6	−166.07 (7)
C5—N1—C2—C3	179.48 (7)		

Hydrogen-bond geometry (Å, º)

D—H···*A*	*D*—H	H···*A*	*D*···*A*	*D*—H···*A*
N3—H3*A*···O1^{i}	0.89 (1)	2.16 (1)	3.0002 (9)	156 (1)
N3—H3*B*···N2^{ii}	0.90 (1)	2.10 (1)	2.9854 (10)	169 (1)

C3—H3···O1^{i}	0.95	2.56	3.3036 (10)	135
C7—H7···O1^{iii}	0.95	2.37	3.2559 (11)	156

Symmetry codes: (i) x, y, $z-1$; (ii) $-x+2$, $-y+1$, $-z+1$; (iii) $x-1$, $-y+1/2$, $z-1/2$.